EVS30 Symposium
Stuttgart, Germany, October 9 - 11, 2017

A control strategy for a smooth engine start in a power-split hybrid electric vehicle

Jianwu Zhang, Donghao Liu *, Defeng Xu, Haisheng Yu, Benben Chai

* *School of Mechanical Engineering, State Key Laboratory for Mechanical Systems and Vibration, Shanghai Jiao Tong University, Shanghai 200240, People's Republic of China. Email: liudonghao@sjtu.edu.cn*

Summary

Engine start-stop technology is significant in reduction of fuel consumption and exhaust pollution especially for hybrid electric vehicles. On the other hand, however, it also deteriorates drive smoothness and ride comfort. By insight into the power-split hybrid vehicles, the engine is directly connected to the transmission and driving wheels without any clutch in the driveline. Therefore, it is difficult to make a trade-off between the engine start and vehicle drive smoothness at the same time. For alleviation of the longitudinal impacts and jerks, the power-split hybrid driveline is numerically modelled counting for the torsional damper stiffness nonlinearities, planetary gear phase uncertainties and engine torque time-varying properties. Accordingly, a fundamental control strategy is developed to coordinate dynamic torques of the engine and motors from time to time during the engine starts. In fact, the hybrid passenger car undergoes shuffles and jerks due to severe torsional vibrations, most of which are a series of low-order modal resonances of the hybrid driveline. For reducing vibrations stimulated during the period of engine starts, active damping methods are adopted to compensate the engine torque fluctuations. By simulation results for vibration depressions of the hybrid driveline and vehicle, it is shown that the active damping strategy counting for elastic properties of the torsional damper is efficient.

Keywords: Hybrid electric vehicle, engine start-stop excited vibrations, deep hybrid transmission, active damping control, motor torque coordination control.

1 Introduction

Deep hybrid electric vehicles matched with power-split planetary gear transmissions are common recognized to be an efficient solution in the transitional stage of oil litre-mileage regulations, by which battery and regenerative energies are efficiently utilized and engine operation time is reduced by more than 50% in comparison with conventional vehicles [1]. Automatic engine start-stop control is one of fundamental means for HEVs in oil saving and exhaust reduction. However, frequent start-stop induced shocks would certainly deteriorate drive smoothness and ride comfort [2].

Due to different powertrain architectures of HEVs, for instance, series, parallel, and power-split hybrids, the relevant start-stop techniques are quite different. In parallel and series HEVs, integrated starter generator (ISG) and belt starter generator (BSG) modules are adopted, in which one or more clutches must be inserted in the driveline to separate the engine power from the HEV during the engine start process. Once the engine starts to work, a soft switch-on of engine power to the driveline requires difficult controls of the clutch engagements [3-6]. However, there exists no such a clutch in the power-split type HEVs between the engine and the driveline.

During the engine start, sudden step inputs of the engine torque directly cause unexpected vibrations of the driveline and the vehicle. As low frequency eigenmodes exist in the hybrid driveline, torsional vibrations are easily stimulated by start-stop processes like the engine sweep-frequency excitations. It is worth noting that all these vibrations and shocks take place without announcement in advance. Therefore, it becomes a challenge to achieve a smooth engine start-stop in the power-split type HEVs.

In the present research, a lumped parameter modelling method is applied for numerical analysis of dynamic performance of a novel power-split HEV to accurately simulate the dynamic system. In particular, the dynamic model of the engine output torques is also developed by means of experiments and analytical methods. According to the reduced driveline model, the torque coordination controller is proposed for a fundamental engine start strategy, and some active damping controls are presented to be a countermeasure against unexpected vibrations during the engine start.

2 Problem descriptions

The novel power-split HEV is synergistically powered by an internal combustion engine (ICE) and two electric motors (E1 and E2), and the hybrid transmission and the driveline are presented in Figure 1. The three power sources are coupled together by the compound planetary gear set, four central members of which are planetary carrier (C), small sun gear (S1), large sun gear (S2) and ring gear (R), respectively. ICE is connected to C as a power input of the transmission by a torsional damper (TD) without clutch, E1 and E2 are connected to S1 and S2, and R is connected to final reduction gear (FR), differential (DF), half shafts (HS) and front wheels (W).

The engine start-stop events in HEVs depend on vehicle speed, battery SOC, driver torque demand, that is, drive conditions of the vehicles are different during the engine starts, for example, standstill, launch, acceleration or cruise. Whenever the engine is started, the traction force is independent from the engine power. For limitation of paper length, only one case is considered that the standing engine starts and the vehicle is at a standstill. As shown in Figure 2, the balance lever [7] graphically represents the whole process of the standing engine start, being divided into four phases, respectively, engine standing phase, preparation phase, crank driven phase and engine ignition phase.

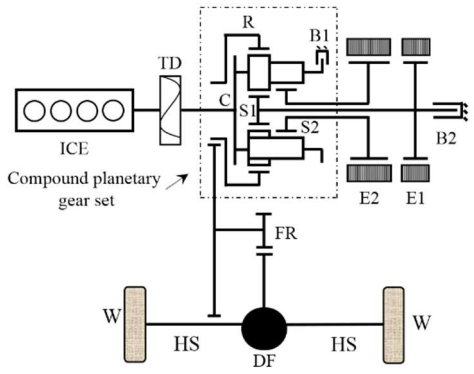

Figure 1. Configuration of the power split hybrid powertrain.

Before the engine starts, as shown in Figure 2(a), B1 is locked as well as E1 and E2 are both in standby. In the preparation phase, as shown in Figure 2(b), B1 is unlocked firstly no sooner when the hybrid control unit (HCU) decides to start the engine. Further in the crank driven phase, as shown in Figure 2(c), E1 is operated to provide a positive torque for the engine to speed up as quick as possible and E2 is also operated to provide a positive torque for the planetary gear set to keep the ring gear in standstill. The engine is once driven to the idle speed, it begins to work by ignitions. In the steady ignition phase, as illustrated in Figure 2(d), the ICE output torque is utilized for E1 as a generator to charge the battery and meaning while E2 is switched on to provide a negative torque for the planetary gear set to make a balance of the lever. This is also called idle speed charge mode. Though ICE, E1 and E2 are coordinated to work together, the ring gear and the vehicle are always kept in standstill.

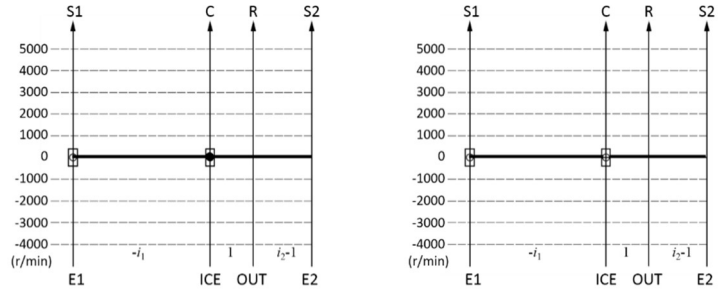

(a)Standstill electric drive mode (b) Preparation phase

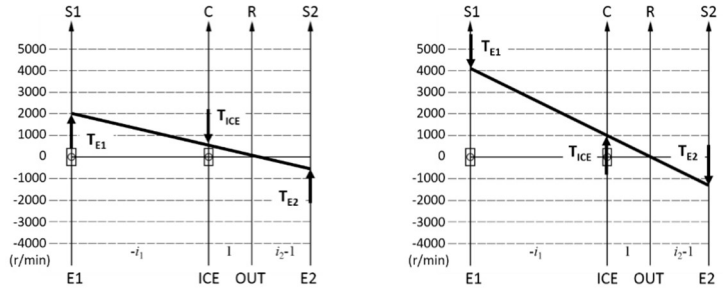

(c)Crank driven phase (d) Ignition phase

Figure 2. The lever diagram during the engine start process

3 Model development

3.1 Dynamic model of the driveline

As shown in Figure 3, a lumped dynamic model of the driveline is accurately constructed in Simulink/Simscape environment.

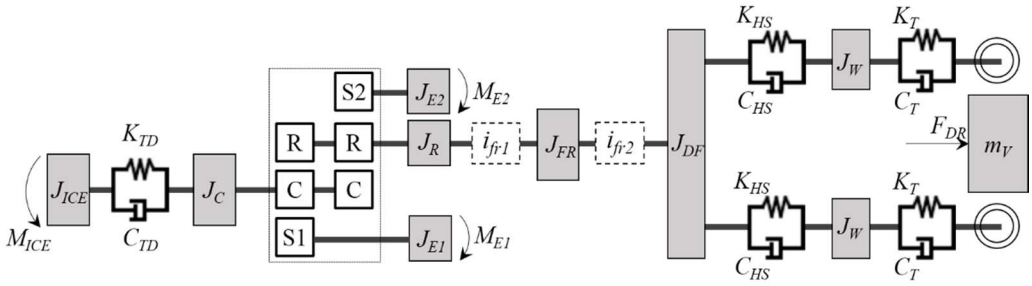

Figure 3. The dynamics model in Simulink for the hybrid driveline and vehicle.

By assuming that the crankshaft is rigid, the crank-rod mechanism including moving pistons, connecting rods, crankshaft and fly wheel can be lumped to be a part having moment of inertia J_{ICE}, to which the engine torque is applied. The moment of inertia Jc are then comprised of those of the planetary carrier and planets. J_{E1} is an equivalent sum of moments of inertia of S1 and E1 rotor, J_{E2} is an equivalent sum of moments of inertia of S2 and E2 rotor, and J_R is moment of inertia of the ring gear. The output torques of E1 and E2 act on J_{E1} and J_{E2}.

By ignoring elastic effects in the final reduction gears, the differential planets and the drive wheels, moments of inertia of the rigid bodies are J_{FR}, J_{DF} and J_W, respectively. In addition, the final reducer includes two-stage of gear reductions and the two gear ratios are i_{fr1} and i_{fr2}. F_{DR} is the drive force including relative aerodynamic drag and rolling resistance.

The dynamic model of the hybrid driveline is comprised of five elastic-damping elements, a torsional damper, two half shafts and two drive wheels. Furthermore, as shown in Figure 4, the TD is characterized of nonlinear stiffness properties, influence of which on transient responses of the driveline is obvious during the engine start .

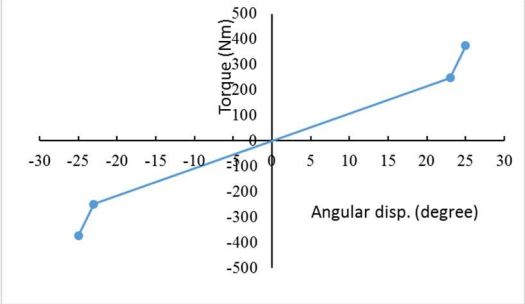

Figure 4. Piecewise linear stiffness properties of the torsional damper.

3.2 Dynamic model for the engine torque

For an accurate model of the gasoline engine torques, therefore, a combination method is proposed with the help of engine experimental results, in which pressures on the piston and corresponding torques to the crankshaft and flywheel are emphasized in particular.

3.2.1 Kinematics of the piston-crank mechanism

The moving element consisting of rods and pistons is one of the first vibration sources of the reciprocating engine. Assume that the origin of coordinates is fixed on the top dead center (TDC), as shown in Figure 5. The displacement of a piston in correspondence to the crank angle α can be described as follows

$$S(\alpha) = r(1-\cos\alpha) + l(1-\sqrt{1-\lambda^2\sin^2\alpha}) \tag{1}$$

Where r is half of the piston stroke, l is length of the connecting rod, and the aspect ratio $\lambda=r/l$.

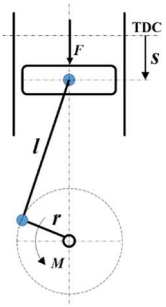

Figure 5. The piston and the crank-rod mechanism.

According to the binomial expansion theorem for the square root expression, the piston position in Equation (1) can be approximated by ignoring higher order terms in the following form as

$$S = r\left[(1-\cos\alpha) + \frac{\lambda}{4}(1-\cos 2\alpha)\right] \tag{2}$$

Whenever the crankshaft is operated at a constant speed, the crank angle α can be expressed in terms of t as

$$\alpha = \omega t = \frac{n\pi}{30}t \tag{3}$$

Where ω is constant angular velocity of the crankshaft, rad/s and n is constant revolution speed of the crankshaft, r/min. By taking the first and second derivatives of the piston displacement in Equation (2) and (3) with respect to time, the piston acceleration may be written as follows

$$\ddot{S} = r\omega^2(\cos\omega t + \lambda\cos 2\omega t) \tag{4}$$

Further according to the equilibrium condition, the total force F acting on the piston is in correspondence to the torque applied to the crankshaft

$$M = FrK \tag{5}$$

Where K is the conversion coefficient between force and torque in the piston-crank mechanism and may be presented of the following form as

$$K = \frac{\sin(\alpha+\beta)}{\cos\beta} = \sin\alpha + \lambda\frac{\sin\alpha\cos\alpha}{\sqrt{1-\lambda^2\sin^2\alpha}} \approx \sin\alpha + \frac{\lambda}{2}\sin 2\alpha \tag{6}$$

3.2.2 Thermal torque

Sudden variations of the cylinder pressure appear once ignition and combustion generate torque ripples of the crankshaft. The engine torque may be expressed below for a single cylinder to be a function of the engine geometry

$$M_g = F_g rK = \frac{\pi D^2}{4}(p_g - p')rK \tag{7}$$

Where F_g is combustion force applied to the piston, D represents diameter of the cylinder, p_g and p' are in-cylinder thermal pressure and the back pressure. In the engine driven phase, p_g is just the air pressure and the corresponding torque is a resistant one. On contrast in the engine ignition phase, p_g is generated by combustion, the corresponding torque is a drive torque.

In Figure 6(a), cylinder pressures versus crank angle are plotted with different engine speeds of 100, 500 and 900 r/min in the engine driven phase. In the engine ignition and injection phase at idle speed, the engine is operated to drive the generator to charge the battery. Test results for the cylinder pressures are obtained and given in Figure 6(b). As a matter of fact, the transition state from the engine driven to steady idling phases is complicated, because the cylinder pressures in each of combustion strokes are different.

For simplicity, inertial effects of connecting rods and crankshaft, the piston inertial torque for a single cylinder may be described in the following form as

$$M_m = (-m_p\ddot{s})rK = -m_p r^2\omega^2(\cos\omega t + \lambda\cos 2\omega t)K \tag{8}$$

where m_p represents mass of a single piston. The inertial torque increases quadratically with the engine speed.

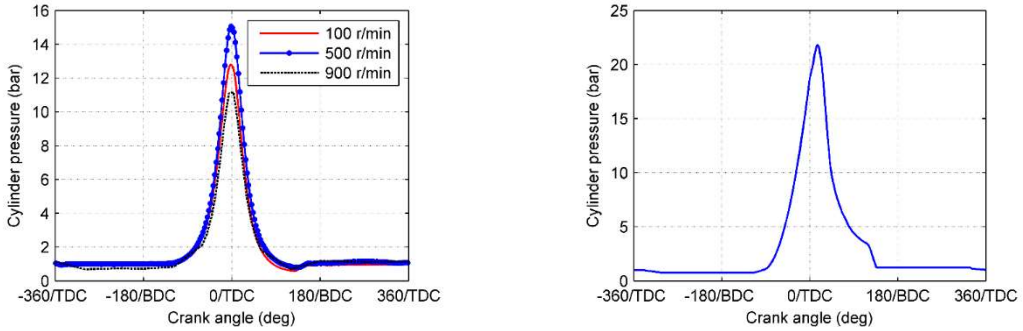

(a)Cylinder pressure at different engine speeds of 100, 500, 900 r/min (b) Cylinder pressure while ignition

Figure 6. Cylinder pressure against crank angle.
BDC: bottom dead center; TDC: top dead center.

3.2.3 Friction torque

By ignoring waves of the friction torque and the temperature influence, the simplified friction torque formulation is suggested and expressed by Heywood [8] in terms of engine speed for four-stroke gasoline engines in the following form as

$$M_f = f_0 + f_1 n + f_2 n^2 \tag{9}$$

Where f_0, f_1 and f_2 are polynomial coefficients to be determined. Experimental results for the friction torques are measured by bench test at different operation speeds are plotted in Figure 7, and quadratic polynomial fitting curve is also determined according to Eq. (9).

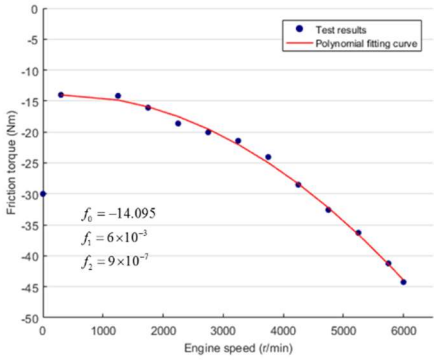

Figure 7. Test measures for the total friction losses in pure electric drive mode.

3.2.4 Torque responses of a four-cylinder engine

A simple block diagram is shown in Figure 8 for the torque model, inputs of which are cylinder pressures, angular positions and crankshaft speed.

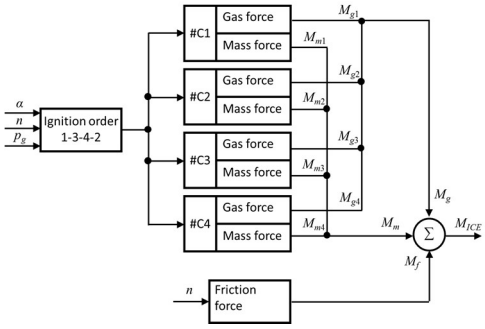

Figure 8. The dynamic model for engine torques.

In Figures 9(a) and (b) numerical results are plotted for the engine driven torques against the crank position in electric drive mode and engine operation mode. As observed from Fig.9, the dynamic response of engine torques appear periodically and the frequency of the engine torques is exactly two times that of the engine speeds.

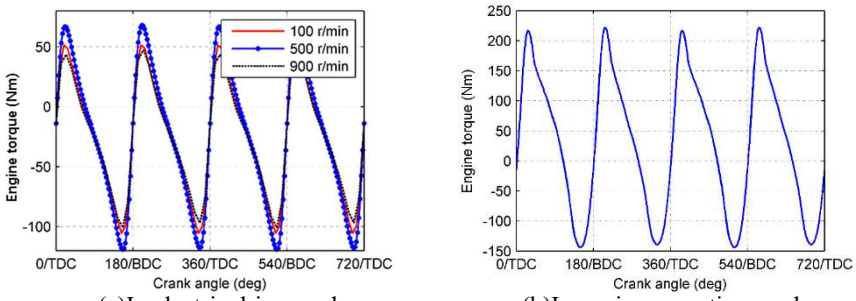

(a)In electric drive mode (b)In engine operation mode

Figure 9. Dynamic responses of the engine torques.

4 Fundamental control design for engine starts

4.1 Driveline simplification and modelling

As shown in Figure 10, the moments of inertias of the two motors are the same as in the full driveline model. J'_C is total moment of inertia of rotational components from the engine to carrier, J'_R is equivalent moment of

inertia of rotational components from the ring gear to the car body. The formulations of J'_C and J'_R can be presented below

$$J'_C = J_{ICE} + J_C \tag{10}$$

$$J'_R = J_R + \frac{J_{FR}}{i_{fr1}^2} + \frac{J_{DF} + 2J_W + Mr_t^2}{i_{fr1}^2 i_{fr2}^2} \tag{11}$$

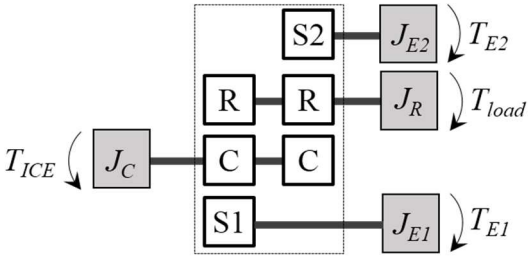

Figure 10. The simplified model for control development.

4.2 Dynamic control of engine torques

The equilibrium equations of the simplified dynamics model of four degrees of freedom may be expressed of the following form as

$$J_{E1} a_{S1} = T_{E1} - T_{S1} \tag{12}$$

$$J_{E2} a_{S2} = T_{E2} - T_{S2} \tag{13}$$

$$J'_C a_C = T_{ICE} - T_C \tag{14}$$

$$J'_R a_R = T_R - T_{load} \tag{15}$$

where α_{S1}, α_{S2}, α_C and α_R are angular accelerations of S1, S2, C and R, T_{S1}, T_{S2}, T_C and T_R are torques applied to S1, S2, C and R, T_{E1} and T_{E2} are driving torques of E1 and E2, T_{lCE} is the engine output torque determined directly by the engine management system (EMS), T_{load} is equivalent torque to longitudinal inertia loading of the hybrid vehicle. Furthermore, it should be noted that T_{lCE} is used to be a control variable and determined by MVEM and M_{lCE} is transient engine torque used in the vibration control as soon as the engine starts and stops.

Motion constraints of the four angular accelerations are derived out accordingly by the compound planetary gear set and can be written up as follows

$$a_{S1} = a_R \cdot i_1 + a_C \cdot (1 - i_1) \tag{16}$$

$$a_{S2} = a_R \cdot i_2 + a_C \cdot (1 - i_2) \tag{17}$$

Where i_1 and i_2 are stationary ratios of planetary gear sets subject to single-planet and double-planet gear system, respectively.

Equilibrium equations of torques in the planetary gear set may be also presented below

$$T_C + T_R + T_{S1} + T_{S2} = 0 \tag{18}$$

$$T_R + T_{S1} \cdot i_1 + T_{S2} \cdot i_2 = 0 \tag{19}$$

By neglecting efficiency losses in the battery pack and DC/AC inverter, the battery power can be expressed in terms of drive motor velocities of the following form as

$$P_B = T_{E1}\omega_{E1} + T_{E2}\omega_{E2} \tag{20}$$

Where P_B is battery power, ω_{E1} and ω_{E2} are angular velocities of E1 and E2, respectively.

By far the controller for the engine transient torques can be constructed by Equations (12) to (20). Moments of inertias, material properties and stationary ratios are known and listed in Table 1. In addition, rotational speeds of the electric motors can be measured by their electric resolvers in time. However, there are 13 unknown variables in the set of 9 algebraic equations. Once 4 of the unknowns are specified, the other variables can be solved. Therefore, by knowing a_R, a_C, T_R and T_{ICE}, starting torques of E1 and E2 can be obtained by solving the algebraic equations in the matrix form as

$$\begin{bmatrix} J_{E1} & 0 & -1 & 0 & 0 & 1 & 0 & 0 & 0 \\ 0 & J_{E2} & 0 & -1 & 0 & 0 & 1 & 0 & 0 \\ 0 & 0 & 0 & 0 & 0 & 0 & 0 & 1 & 0 \\ 0 & 0 & 0 & 0 & 1 & 0 & 0 & 0 & 0 \\ 1 & 0 & 0 & 0 & 0 & 0 & 0 & 0 & 0 \\ 0 & 1 & 0 & 0 & 0 & 0 & 0 & 0 & 0 \\ 0 & 0 & 0 & 0 & 0 & 1 & 1 & 1 & 0 \\ 0 & 0 & 0 & 0 & 0 & i_1 & i_2 & 0 & 0 \\ 0 & 0 & -\omega_{S1} & -\omega_{S2} & 0 & 0 & 0 & 0 & 1 \end{bmatrix} \bullet \begin{bmatrix} a_{S1} \\ a_{S2} \\ T_{E1} \\ T_{E2} \\ T_{load} \\ T_{S1} \\ T_{S2} \\ T_C \\ PB \end{bmatrix} = \begin{bmatrix} 0 \\ 0 \\ T_{ICE} - J'_C a_C \\ T_R - J'_R a_R \\ a_R i_1 + a_C (1 - i_1) \\ a_R i_2 + a_C (1 - i_2) \\ -T_R \\ -T_R \\ 0 \end{bmatrix} \tag{21}$$

In the engine drive phase, the engine outputs powers to drive two motors for electricity generation and battery pack charge according to the SOC. At this moment, all the power sources work in a steady state and accelerations of the engine and motors are zero. By these values, torques of E1, E2 and engine can be solved by the algebraic equations in matrix form as formula 22.

$$\begin{bmatrix} J_{E1} & 0 & -1 & 0 & 0 & 0 & 1 & 0 & 0 \\ 0 & J_{E2} & 0 & -1 & 0 & 0 & 0 & 1 & 0 \\ 0 & 0 & 0 & 0 & 0 & -1 & 0 & 0 & 1 \\ 0 & 0 & 0 & 0 & 1 & 0 & 0 & 0 & 0 \\ 1 & 0 & 0 & 0 & 0 & 0 & 0 & 0 & 0 \\ 0 & 1 & 0 & 0 & 0 & 0 & 0 & 0 & 0 \\ 0 & 0 & 0 & 0 & 0 & 0 & 1 & 1 & 1 \\ 0 & 0 & 0 & 0 & 0 & 0 & i_1 & i_2 & 0 \\ 0 & 0 & \omega_{S1} & \omega_{S2} & 0 & 0 & 0 & 0 & 0 \end{bmatrix} \bullet \begin{bmatrix} a_{S1} \\ a_{S2} \\ T_{E1} \\ T_{E2} \\ T_{load} \\ T_{ICE} \\ T_{S1} \\ T_{S2} \\ T_C \end{bmatrix} = \begin{bmatrix} 0 \\ 0 \\ -J'_C a_C \\ T_R - J'_R a_R \\ a_R i_1 + a_C (1 - i_1) \\ a_R i_2 + a_C (1 - i_2) \\ -T_R \\ -T_R \\ PB \end{bmatrix} \tag{22}$$

The block diagram of the torque controller is developed based on models and tests and shown in Figure 11. The engine starts are triggered in simulations by the calibration of battery SOC. Once HCU receives directories to start the engine, the hydraulic valve plate (HVP) first responses to control the brakes and clutches in the hybrid transmission. By the torque controller, demand torques of the engine and motors are then computed and the three power sources are operated by EMS and power electronic units (PEUs) to assign the actual torques. Furthermore, the calibrated SOC is appliable for the engine ignition model whenever required.

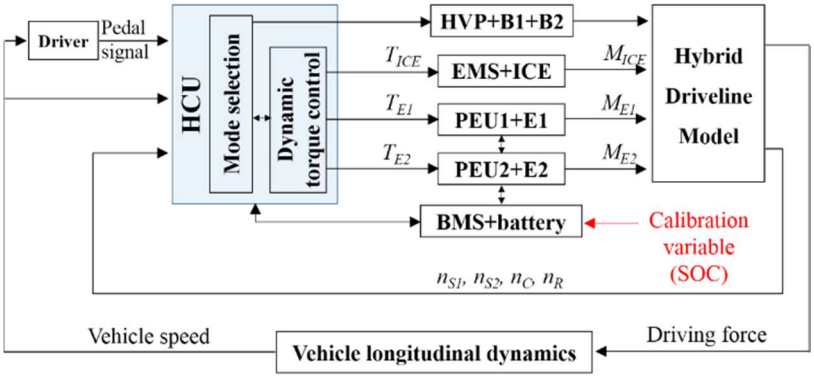

Figure 11. The block diagram of the torque controller for the model-based functional test.

4.3 Simulation results and analysis

A simulation analysis for the engine starts is performed to evaluate efficiency of the controller and effectiveness of the driveline impact reduction. Numerical results of transient speed and torque responses are plotted in Figure 12, as shown clearly, the process of the engine starts in ranges from 0.2 to 0.7 s and then the engine begins to operate in order. Obviously, the engine start process takes very short time and is completed by the engine torque controller.

As seen in Figure 12(a), since the torsional damper and the static engine friction play effective roles, the speed of the planetary carrier is higher than the engine speed at the earlier stage in the engine driven phase, and the

engine speed increases quickly and fluctuates severely. The vibrations further induce self-excited resonance of the whole driveline. After ignitions, the engine speed tends to keep constant more or less in a small range of ±50 r/min. At the same time, speed fluctuations of the engine and carrier are filtered by the torsional damper and the carrier speed responses behave much smoother than before.

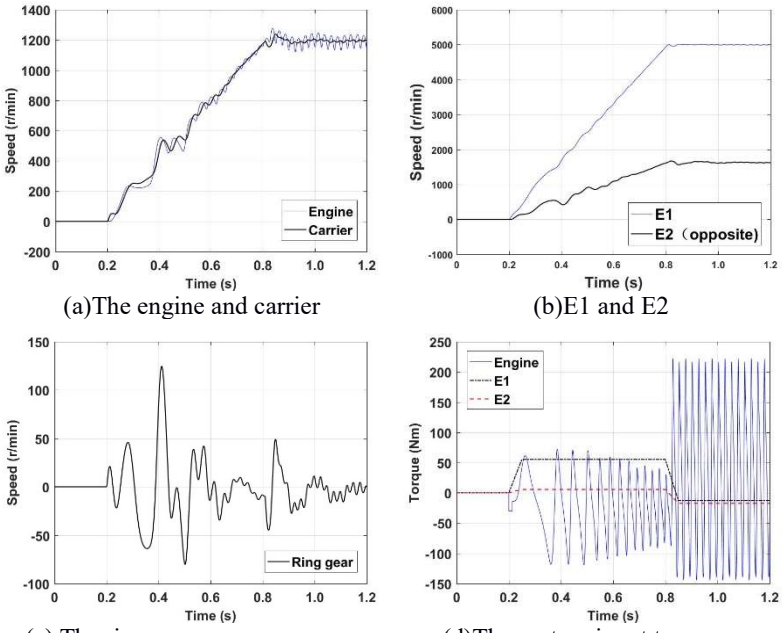

(a)The engine and carrier (b)E1 and E2

(c) The ring gear (d)The system input torques

Figure 12. Simulation results of transient speed and torque responses by the fundamental control during the engine start.

As seen from Figure 12(b) and (c), the most severe fluctuations of the speed responses of E1, E2 and the ring gear also occur in the engine driven phase. The maximum peak-to-peak value of the ring gear speed response is more than 188 r/min and the corresponding engine speed is about 400 r/min, at which severe fluctuations cause vehicle jerks and deteriorate drive and ride comforts. In addition, as also observed from Figure 12(c), the engine ignition in the very beginning also causes shocks in the driveline at 0.7 s. However, the shock induced vibrations are not considered in the present research, because initial combustions can be controlled to be smooth by optimizations of EMS ignition module. During the steady ignition phase, the self-excited resonant vibrations of the ring gear are measured to be really small with respect to the maximum peak-to-peak value of 20 r/min.

Actually, torsional vibrations in the engine crank driven phase imply mainly the presence of resonances in the driveline, because the engine excitations during the engine start process are large amplitude and wideband vibrations in output torques, as shown in Figure 12(d). As shown in Figure 13, the engine speed is accelerated from 0 to 2100 rpm and this process like a sweep-frequency excitation from 0 to 35 Hz to the driveline with low-order natural frequencies 6.2, 14.3 and 22.7 Hz. The second order excitation of the engine coincides with the natural frequency 14.3 Hz of the driveline while the engine crank is driven just at 420 r/min, corresponding to the modal vibrations of the ring gear and close to the engine speed 400 r/min mentioned before.

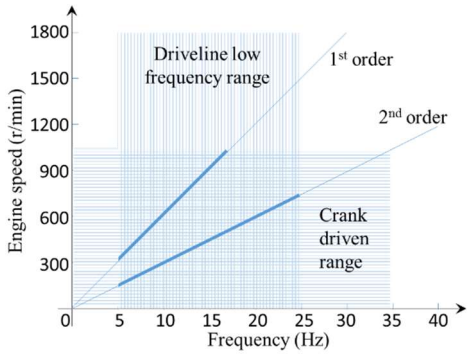

Figure 13. Comparison of the driveline low natural frequency range with the engine excitations sweep frequency range.

5 Active damping control of transient vibrations

5.1 Active damping controller design

For the first case only the engine speed sensor is chosen and applied to estimate the engine output torque, so called engine-sensor-based active damping controller (ESB-ADC). As shown in Figure 14, the engine output torque is directly given according to the model-based map of the engine by the flywheel speed and crankshaft position sensors. The engine model-based map is obtained from the dynamic model of the engine torque in the motor drive mode. Compensation torques for the two motors are computed by the dynamic torque controller in Equation (21). The compensation and starting torques for the two motors are added up and then applied to the driveline. In this case, besides the estimated engine torque, the inputs of the dynamic torque controller, a_C, a_R, and T_R, are all set to zero and then the solution of Equation (21) is only associated with the compensation torques.

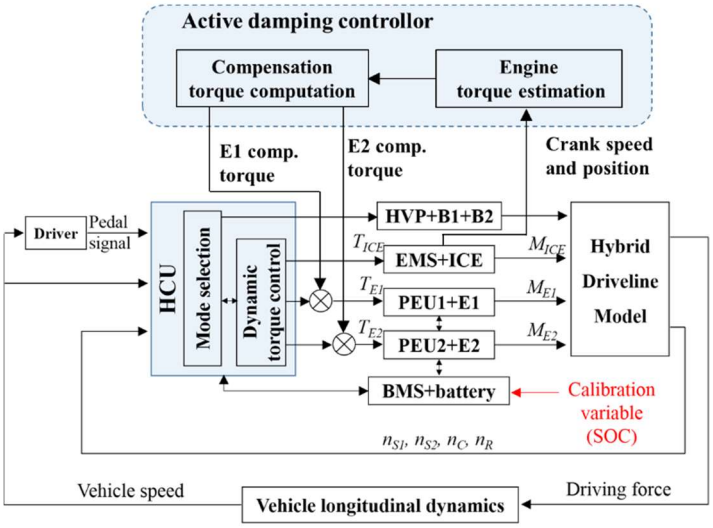

Figure 14. The block diagram of ESB-ADC.

For the second case, the engine and motor position sensors are employed to estimate the carrier torque, so called engine-and-motor-sensors-based active damping controller (EMSB-ADC). As shown in Figure 15, the estimated engine torque in ESB-ADC is replaced by the torsional damper torque evaluated by positions of the flywheel and the carrier and nonlinear stiffness properties of the TD. The carrier position is computed by the resolvers of motors.

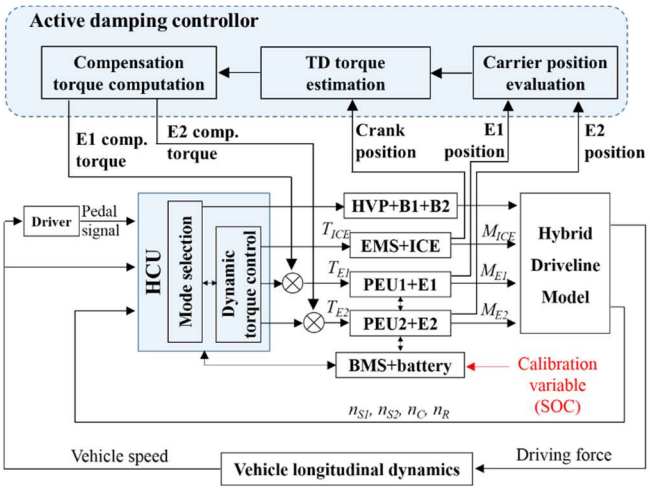

Figure 15. The block diagram of EMSB-ADC.

The compensation torque computation is equivalent to the solution of Equation (21), in which the notation T_{ICE} is replaced with the torsional damper torque estimated in this controller. Moreover, a_C, a_R, and T_R are also set to zero as in the ESB-ADC and the compensation torques are obtained only by solving the set of algebraic

equations. Consequently, the compensation and engine start torques for two motors are added up and imposed to the driveline.

5.2 Simulation results and comparison

The two active damping controllers are implemented in the dynamic system of the driveline and simulation results of transient torque responses for the carrier, ring gear and two motors are plotted in Figure 16. The dynamic performances of the control system by the three control methods are compared and listed in Table 2.

As seen from Fig.16 (a), the engine can be driven smoothly to start by implementation of the active damping controllers. In comparison of simulation results by three control strategies, the effect of ESB-ADC is slightly negative on reducing resonant vibrations of the driveline in the engine crank driven phase. As shown in Figure 16 (b) and Table 2, the ring gear speed responses oscillate in large-amplitude with a maximum peak-to-peak value of 210 r/min larger than that of 188.4 r/min by the fundamental control. Since stiffness properties of the torsional damper are not considered in the feed forward control, the compensation torques are delayed too much to eliminate the engine shocks by the superposition principle. Even a worse consequence is observed. The negative effect of the control occur when the compensation torque responses have the same phase of the engine torques.

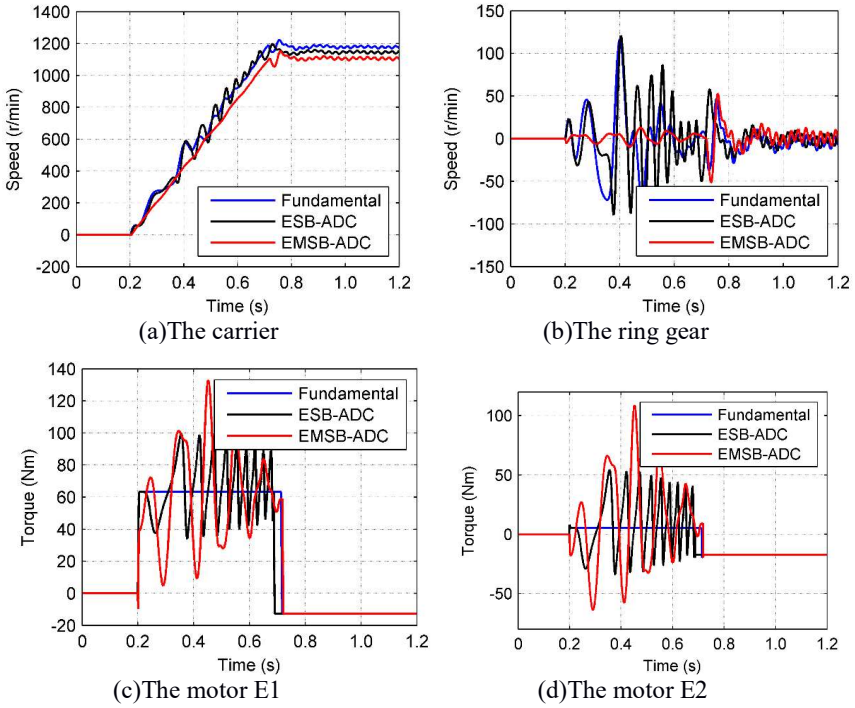

(a)The carrier (b)The ring gear

(c)The motor E1 (d)The motor E2

Figure 16. Comparisons of numerical results of speed and torque response by the active damping controls with those by the fundamental control.

In order to solve the problem of no effect of ESB-ADC on reducing the torsional vibrations, such a bypass clutch is used to establish a rigid connection between the transmission and the engine that effects of the torsional damper during the engine start are avoided for GM 2-mode HEV [9].

Table 2. Comparison of performance by three control methods.

control system	maximum amplitude of ring gear speed (r/min)	maximum peak-to-peak value of ring gear speed (r/min)
Fundamental control	116.5	188.4
ESB-ADC	120.7	210.0
EMSB-ADC	12.8	22.0

By comparisons of simulation results, it is shown that the technique of EMSB-ADC is effective and efficient in the control of torsional vibrations. As a result, fluctuations of the ring gear speed response attenuate fast in

amplitude to 20 r/min in the engine ignition phase. By the control of compensation torques, it is shown in Figure 16 (a) that the carrier speed responses behave smoothly within a small amplitude of fluctuations in the crank driven phase. Since the carrier torque in EMSB-ADC is considered rather than the engine torque, though the compensation torque delays a little, effect of the active damping control strategy is remarkable.

6 Conclusion

For depression of self-resonant vibrations of the drivetrain in the engine crank driven phase, the whole control strategy is developed, being involved with active damping techniques, existing sensors and feed forward control method. The key idea of the active damping control is associated with a couple of drive motors in the hybrid transmission. The quick responses of the two drive motors are beneficial and the motors act as actuators to compensate the engine torque fluctuations. Accordingly, the engine-sensor-based and engine-and-motor-sensor-based active damping controllers (ESB-ADC and EMSB-ADC) are designed. By simulation results, it is shown that EMSB-ADC is of remarkable capability in reduction of the maximum peak-to-peak value of transient speed responses for the ring gear from 200 to 20 r/min. On contrast, because effect of elastic elements in the torsional damper is not considered, the compensation torques from ESB-ADC are delayed so much that the engine torque fluctuations are intensified. By comparisons of numerical results of speed responses for the carrier, ring gear and motors, only proper active damping control can be used to attenuate transient vibrations in the hybrid powertrains successfully.

7 Funding

This research work is financially supported by the National High Technology Research and Development Program (863) of China under Grant No. 2011AA11A207.

8 References

[1] Reynolds C and Kandlikar M. How hybrid-electric vehicles are different from conventional vehicles: the effect of weight and power on fuel consumption. Environmental Research Letters. 2007; 2: 014003.

[2] Guo R, Cao C, Mi Y, et al. Experimental investigation of the noise, vibration and harshness performances of a range-extended electric vehicle. Proceedings of the Institution of Mechanical Engineers, Part D: Journal of Automobile Engineering. 2015.

[3] Smith A, Bucknor N, Yang H, et al. Controls Development for Clutch-Assisted Engine Starts in a Parallel Hybrid Electric Vehicle. SAE Technical Paper 2011-01-0870, 2011.

[4] Kum D, Peng H and Bucknor NK. Control of Engine-Starts for Optimal Drivability of Parallel Hybrid Electric Vehicles. Journal of Dynamic Systems, Measurement, and Control. 2013; 135: 021020.

[5] Pisu P, Koprubasi K and Rizzoni G. Energy Management and Drivability Control Problems for Hybrid Electric Vehicles. Decision and Control, 2005 and 2005 European Control Conference CDC-ECC '05 44th IEEE Conference on. 2005, p. 1824-1830.

[6] Li C, Gang X and Jing S. Torque Coordination Control During Mode Transition for a Series-Parallel Hybrid Electric Vehicle. Vehicular Technology, IEEE Transactions on. 2012; 61: 2936-2949.

[7] Benford HL and Leising MB. The Lever Analogy: A New Tool in Transmission Analysis. SAE Technical Paper 810102, 1981.

[8] Kuang ML. An investigation of engine start-stop NVH in a power split powertrain hybrid electric vehicle. SAE Technical Paper 2006-01-1500, 2006.

[9] Hwang H-Y. Minimizing Seat Track Vibration That is Caused by the Automatic Start/Stop of an Engine in a Power-Split Hybrid Electric Vehicle. Journal of Vibration and Acoustics. 2013; 135: 061007.